Optimized structures and electronic properties of alkali-metal (Na, K) -adsorbed Si(001) surfaces

K. Kobayashi
National Institute for Research in Inorganic Materials, Namiki 1-1, Tsukuba-shi, Ibaraki 305, Japan

Y. Morikawa and K. Terakura
Institute for Solid State Physics, University of Tokyo, Roppongi, Minato-ku, Tokyo 106, Japan

S. Blügel
Institut für Festkörperforschung, Forschungszentrum Jülich, D-5170 Jülich, Germany
(Received 21 August 1991)

The Na and K adsorption on the Si(001)-2×1 surface is studied by first-principles molecular dynamics based on the norm-conserving pseudopotential. The stable adsorption sites are determined for full coverage ($\Theta=1.0$) and half coverage ($\Theta=0.5$). At $\Theta=0.5$, the configuration with Na and K adsorbed along the trough is more stable than predicted by the Levine model. The coverage dependence of the absorption energy suggests that the saturation coverage should be $\Theta=1.0$ for both Na and K and that a qualitative difference between Na and K can be observed in the growth mode of the adsorbed layer. Supplementary calculations for $\Theta=\frac{1}{3}$ and $\frac{5}{6}$ are performed in order to obtain an insight into the difference between Na and K in the coverage dependence of the adsorption energy. It is pointed out that the partial core correction for the pseudopotentials of Na and K is very crucial in the structural stability arguments.

I. INTRODUCTION

The alkali-metal adsorption process has played a particularly important role in surface science. As alkali-metal atoms have simple electronic structures, an understanding of alkali-metal adsorption should be an indispensable first step towards the understanding of chemisorption in general. Besides, the chemically active nature of alkali-metal atoms makes alkali-metal adsorption very attractive in fundamental research as well as in application: Alkali-metal adsorption produces a significant lowering of the work function and activates chemical reactions on surfaces. Alkali-metal adsorption has therefore been intensively studied for decades, both experimentally and theoretically.[1,2] Nevertheless, there is no consensus of some very fundamental aspects of alkali-metal adsorption. For example, the mechanisms of work-function change by alkali-metal adsorption had been interpreted for a long time in terms of charge transfer as suggested by Gurney[3] before detailed electronic-structure calculations demonstrated that the polarized covalent bond is a more appropriate concept in real systems.[4,5]

The situation of alkali-metal adsorption on a Si surface is more complex. As for the basic nature of adsorption, Ciraci and Batra[6] claimed an almost perfect ionic state for alkali-metal adatoms even at high coverage, while Ishida and Terakura[7] demonstrated the existence of strong hybridization between the *s* state of an alkali-metal adatom and substrate Si states and claimed a validity for the polarized covalent-bond picture even at low coverage. In addition to such fundamental problems in the electronic state, structural problems on the Si surface are also of great importance. For specificity, we will confine ourselves to alkali-metal adsorption on the Si(001) surface in the following.

On the clean Si(001) surface, the outermost Si atoms form dimer rows. At the saturation coverage of alkali-metal atoms on this surface, the Levine model,[8] where adatoms are assumed to sit at the hollow site along the hill of the dimer row (called the HH site hereafter), has been widely accepted. The Levine model corresponds to $\Theta=0.5$ with the coverage Θ defined as a ratio of the number of adatoms to that of the outer most substrate Si atoms. The surface must be metallic with $\Theta=0.5$. However, Enta *et al.*[9] found by angle-resolved photoemission measurement that the Si(001) surface with a saturation coverage of K is insulating, and Abukawa and Kono[10] proposed a double-layer model in which K would be adsorbed along the trough between the dimer rows as well as at the HH site. A reflection high-energy electron-diffraction (RHEED) analysis[11] and the thermal-desorption spectrum[12] support the double-layer model. A recent experiment using ion scattering[13] also claims $\Theta=1.0$ to be the saturation coverage. The insulating nature of the surface was also concluded for Na adsorption at saturation coverage,[14] which was taken as evidence of $\Theta=1.0$. However, there are some strong arguments against it. According to an analysis by Glander and Webb,[15] the saturation coverage of Na is $\Theta=0.68$.

After the work by Enta *et al.*[9] and Abukawa and Kono,[10] several theoretical attempts have been made to determine the stable adsorption site for Na and K. (See Fig. 1 for the possible adsorption sites.) At $\Theta=0.5$, Ye, Freeman, and Delley[16] and Ramirez,[17] respectively, identified $T4$ as the K-adsorption site with the shortest

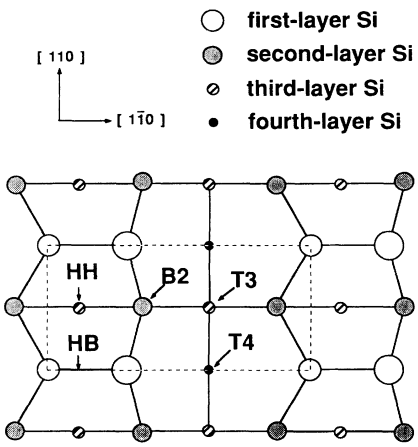

FIG. 1. Top view of the Si(001)-2×1 asymmetric surface. The 2×1 unit cell is indicated by dashed lines. The HH, HB, $T3$, $T4$, and $B2$ sites are indicated. The interdimer bridge site $B2$ is not necessarily just on top of the second-layer Si atom.

K-Si bond lengths of 3.22 and 2.65 Å. In a recent work by Batra on Na adsorption,[18] the original Levine model was supported. Among the three works, the lattice relaxation of the substrate was taken into account only in Batra's work. Ye, Freeman, and Delley treated an extended cluster with the discrete-variational method combined with the local-density approximation (LDA) in density-functional theory; Ramirez, an isolated slab with an incomplete neglect of differential overlap (INDO) scheme of the Hartree-Fock method; and Batra, a repeated-slab model with norm-conserving pseudopotentials in the LDA. Our previous calculation for Na adsorption,[19] similar to Batra's, however, led us to identify $T4$ as the adsorption site, similar to the results by Ye, Freeman, and Delley and Ramirez, but with an energy difference between the HH- and $T4$-site adsorptions of only 0.01 eV/Na. At $\Theta=1.0$, Batra did not find a meaningful energy difference between the two possible combinations of adsorption sites, HH-$T3$ and HH-$T4$, while we found that the combination HH-$T3$ is slightly more stable than that of HH-$T4$ by 0.01 eV/Na.[19,20]

In our recent work,[21] we performed similar calculations on the K/Si(001) system and demonstrated that the optimized structure at $\Theta=1.0$ agrees well with the double-layer model of Abukawa and Kono[10] and that it could explain the thermal-desorption spectrum.[12] Another important lesson from this calculation is that the partial core correction (PCC) (Ref. 22) to K is crucial for obtaining a reasonable K-Si bond length. Without the PCC, the bond length is underestimated. With these findings, we checked the effect of the PCC on Na and found it also to be very important. In Batra's calculation[18] and our previous ones,[19,20] the PCC was not taken into account and the Na-Si bond length was too short compared with the experimental estimate. With the implementation of the PCC, the most stable adsorption site at $\Theta=0.5$ turns out to be the $T3$ site for both Na and K.

The purposes of the present work are to present several theoretical results for both Na and K adsorption and to discuss their implications in order to attain a comprehensive understanding of the structural stability of alkali-metal adsorption on the Si(001) surface. Our results for the coverage dependence of the adsorption energy suggest a qualitative difference between Na and K in the growth mode of the adsorbed layer. A detailed discussion will be given to the microscopic origin of this difference.

The organization of the present paper is as follows: in Sec. II model and methodological details are described. Results are presented in Sec. III, and concluding remarks are given in Sec. IV. Some comments are made on the PCC in the Appendix.

II. MODEL AND CALCULATIONAL METHOD

The present calculation is based on the LDA in density-functional theory[23,24] with the Wigner interpolation formula,[25] for the exchange and correlation, and on the norm-conserving pseudopotential.[26] The pseudopotentials for Si and Na are obtained following the prescription by Bachelet, Hamann, and Schlüter, while the p and d parts of the pseudopotential of K are obtained by Hamann's scheme.[27] The d part is treated as a local potential for all the three elements, and the pseudopotentials are transformed into a separable form as suggested by Kleinman and Bylander.[28] The PCC developed by Louie, Froyen, and Cohen[22] is incorporated into the pseudopotential for Na and K. The PCC is very important for Na and K, although it can be neglected for Si.

We adopt a repeating-slab geometry and a plane-wave basis. The substrate is represented by a ten-layer Si(001) slab, and a vacuum region of the same thickness (13.6 Å) is inserted in between Si slabs. However, for estimating the work function, only the electronic structure is recalculated with a thicker vacuum region of 19.0 Å. The alkali-metal atoms are introduced on each surface of the Si slab. The cutoff energy of the plane-wave basis is 6.25 Ry, which results in a maximum number of 1488 plane waves for $\Theta=0.5$ and 1.0 with the (2×1) unit cell and 4304 plane waves for $\Theta=\frac{1}{3}$ and $\frac{5}{6}$ with the (2×3) unit cell. The surface Brillouin zone is divided into 4×8 (2×2) meshes, and 32 (4) inequivalent K points are used for $\Theta=0.5$ and 1.0 ($\Theta=\frac{1}{3}$ and $\frac{5}{6}$). The optimization of the electronic and ionic degrees of freedom is performed by a modified version of first-principles molecular dynamics (FPMD).[29] We adopt a steepest-descent type of algorithm for the electronic degree of freedom as proposed by Williams and Soler[30] and ordinary molecular dynamics for the ionic motion. The convergence criterion for forces acting on atoms is 3.0×10^{-3} Ry/a_{H}, with a_{H} denoting the Bohr radius (=0.5292 Å). We use the optimized (2×1) asymmetric dimer structure as a starting configuration for the substrate and consider three possible adsorption sites HH, $T3$, and $T4$, as shown in Fig. 1. In our previous calculations,[20] the adsorption at the bridge site of the Si-Si dimer was found to be very unstable. In order to check whether these adsorption sites are local minima on the Born-Oppenheimer surface, the starting positions of Na and K atoms are away from these sites by about 0.48 Å along the dimer row. In the

process of structural optimization, the Si atoms in the two center layers of each Si slab are fixed at their bulk positions for K adsorption, while all the Si atoms are allowed to relax for Na adsorption. As the atomic displacement in the middle layers is only 0.17 Å, the difference in the optimization process between Na and K cases may produce only minor effects.

III. RESULTS AND DISCUSSION

We first describe the effects of the PCC on the bulk cohesive properties of Na, K, and Si. The calculational conditions and results, together with the experimental data,[31–33] are summarized in Table I. Clearly, the PCC is crucial in obtaining reasonable cohesive properties for Na and K, while it has negligible effects for Si. The importance of the PCC for alkali-metal atoms may be interpreted in the following way. First, in the case of K in particular, overlap between the core and valence charges may be significant because of the existence of a rather shallow core state. Second, as the alkali-metal atoms are monovalent, the valence-electron density is rather low. Therefore, the valence-core charge overlap produces relatively significant effects in the exchange-correlation energy and potential. Third, as the alkali metals are soft, a small change in the potential may cause a large change in the cohesive properties. Further comments on the PCC are made in the Appendix.

A. Stable structures

1. *Clean Si(001) surface*

We optimized the structure of the clean Si(001)-2×1 surface with asymmetric dimers. The amount of buckling, i.e., the difference in the height, of the Si atoms of the asymmetric dimer is 0.54 Å and the dimer-bond length is 2.26 Å. The corresponding values by Yin and Cohen[34] are 0.31 and 2.25 Å, respectively. The present bond length is shorter than the experimental value[35] (2.47 Å) by 8.5%. As we show in a separate paper,[36] the optimized value of the dimer-bond length in the $c(4\times2)$ structure is 2.31 Å, which is slightly closer to the experimental value. When alkali-metal atoms are adsorbed with high coverage ($\Theta \geq 0.5$), the asymmetry in the Si-Si dimer is significantly suppressed. Therefore, the ordering energy of the asymmetric dimers will also be suppressed. This will justify the use of the (2×1) unit cell in the present study on alkali-metal adsorption for $\Theta=0.5$ and 1.0.

2. $\Theta=0.5$

Both HH and $T3$ sites are local minima, with the latter being more stable for adsorption of Na and K. Even if the starting atomic position is fairly close to the $T4$ site, both Na and K move toward the $T3$ site. There is experimental evidence supporting our results for K.[37] Note, however, that in our previous calculation[19] for Na without the PCC, $T4$-site adsorption was more stable than $T3$-site adsorption. We will show later that atomic size may be an important factor in determining the stable adsorption site. Side views of the optimized structures are shown in Figs. 2 and 3 and some of the interatomic distances are summarized in Table II. As for the substrate relaxation upon Na or K adsorption, the Si-Si dimer-bond length is significantly elongated and the asymmetry in the Si-Si dimer is reduced. K produces a slightly larger substrate relaxation.

As we demonstrate later, the intersite distance both for the $T3$ and HH sites is too short for K. In this sense, zigzag displacement of K atoms seems to be plausible in order to relax the strain in the adatom chain. Ye, Freeman,

TABLE I. Summary of bulk calculations of lattice constant and bulk modulus for bulk materials Na, K, and Si together with the experimental data. Deviation of the calculated value from the experimental one is shown in the parentheses. "no PCC" and "PCC" denote calculated results without and with the partial core correction, respectively. The cutoff energy for the plane-wave expansion is shown in the parentheses in the first column.

		Lattice constant (Å)	Bulk modulus (Mbar)
Na	no PCC (12.25 Ry)	3.762 (−10.96%)	0.098 (+44%)
	PCC (12.25 Ry)	4.090 (−3.20%)	0.083 (+22%)
	experimental	4.225[a]	0.068[a]
K	no PCC (16.0 Ry)	5.013 (−4.06%)	0.038 (+2.7%)
	PCC (16.0 Ry)	5.132 (−1.78%)	0.041 (+10.8%)
	PCC (6.25 Ry)	5.138 (−1.67%)	0.039 (+5.4%)
	experimental	5.225[b]	0.037[c]
Si	no PCC (12.25 Ry)	5.475 (+0.83%)	0.985 (−0.30%)
	PCC (12.25 Ry)	5.479 (+0.90%)	0.880 (−10.9%)
	no PCC (6.25 Ry)	5.452 (+0.41%)	0.983 (−0.51%)
	experimental	5.430[a]	0.988[a]

[a]Reference 31.
[b]Reference 32.
[c]Reference 33.

TABLE II. Summary of bond lengths (in Å). In the second column, the Si-Si dimer-bond lengths are indicated. In the third to fifth columns, the shortest distances between the Na (K) atom adsorbed at the $T3$ (or HH) site and the first- (or second-) layer Si atom are indicated (ML=monolayer).

			Si-Si dimer	$T3$ first-layer Si	$T3$ second-layer Si	HH first-layer Si
	Clean		2.26			
Na	0.5 ML	($T3$)	2.42	3.28	3.10	
	0.5 ML	(HH)	2.38			2.88
	1.0 ML	(HH-$T3$)	2.63	3.28	3.06	2.97
K	0.5 ML	($T3$)	2.38	3.53	3.39	
	0.5 ML	(HH)	2.38			3.33
	1.0 ML	(HH-$T3$)	2.54	3.47	3.36	3.36

and Delley in fact demonstrated very large zigzag displacement of K atoms for HH-site adsorption and a sizable displacement of about 0.05 a.u., both for zigzag and pairing modes for $T4$-site adsorption.[16] In contrast to this, Batra showed that neither the zigzag nor the pairing displacement could be realized for Na atoms at the HH sites.[18] However, one may wonder whether Batra's conclusion may be affected by the underestimated bond length. Therefore, we reconsidered the possibility of any modification of a linear chain of K atoms, but only for $T3$-site adsorption by using a (2×2) unit cell. According to the present calculation, modification of a straight-linear chain is virtually nonexistent: The amount of displacement is at most 0.004 a.u. in any direction, being one order of magnitude smaller than the value given by Ye, Freeman, and Delley,[16] although the substrate Si-Si

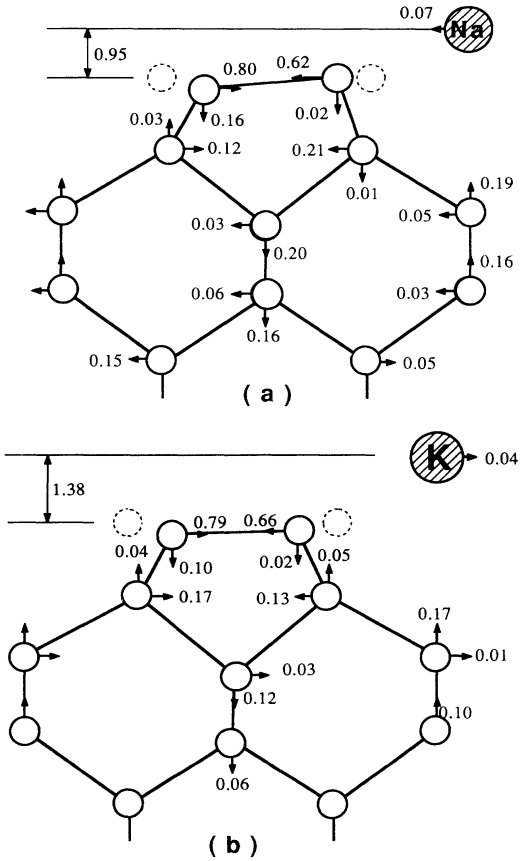

FIG. 2. Side views of the optimized structure for $T3$-site adsorption of (a) Na and (b) K. Displacements from the bulk-terminated ideal surface are indicated in Å. The first-layer Si atoms on the ideal surface are indicated by the dotted circles, with reference to which the height of Na (K) atoms (hatched circles) is measured. The horizontal displacements of Na (K) atoms are measured with reference to the third-layer Si atoms of the ideal surface.

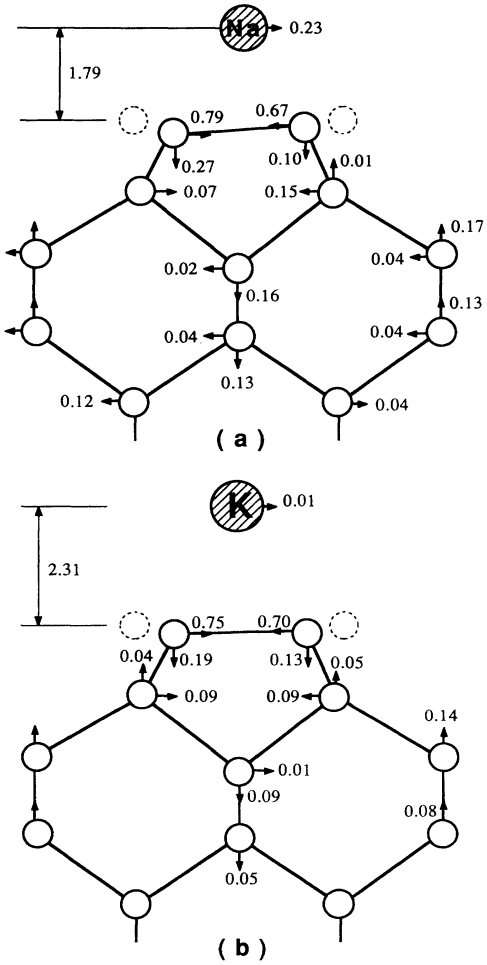

FIG. 3. Side views of the optimized structure for HH-site adsorption of (a) Na and (b) K.

dimers are still weakly asymmetric with an amount of buckling of 0.02 a.u. and are arranged to form a $p(2\times2)$ unit cell.

3. $\Theta=1.0$

The stable configuration is a combination of the HH and $T3$ sites for Na and K. Again, even if we put one Na or K close to the $T4$ site, it moves toward the $T3$ site. We obtained the same result for Na in our previous work[20] even without the PCC. The HH-$T3$ configuration at $\Theta=1.0$ for K is consistent with x-ray photoelectron-diffraction analysis.[10] Side views of the optimized structures are shown in Fig. 4, and the interatomic distances are tabulated in Table II. We note a slight further relaxation of the substrate: the surface Si-Si dimer is now essentially symmetric for both Na and K.

4. $\Theta=\frac{1}{3}$ and $\frac{5}{6}$

These coverages are studied in order to analyze the coverage dependence of the adsorption energy. We start with a configuration for $\Theta=\frac{1}{3}$ ($\Theta=\frac{5}{6}$), where adatoms at every three $T3$ (HH) sites are removed from the $\Theta=0.5$ ($\Theta=1.0$) case, and optimize the structure. Figures 5 and 6 show the top views of the optimized structures for $\Theta=\frac{1}{3}$ and $\frac{5}{6}$, respectively, where the arrows indicate the lateral displacement of adatoms from the ideal HH and $T3$ sites. Note that we do not claim these structures to be the actual ones for $\Theta=\frac{1}{3}$ and $\frac{5}{6}$. Here we are mainly aiming to study the coverage dependence or, equivalently, the coordination-number dependence of the equilibrium interatomic distance. We can readily see in Fig. 5(a) that the Na-Na distance 3.40 Å for $\Theta=\frac{1}{3}$ is much shorter than the intersite distance of the substrate, 3.84 Å, whereas Na atoms are located almost exactly at the high-symmetry adsorption sites for $\Theta=\frac{5}{6}$ in Fig. 6(a). Although these Na-Na distances are affected by the nonuni-

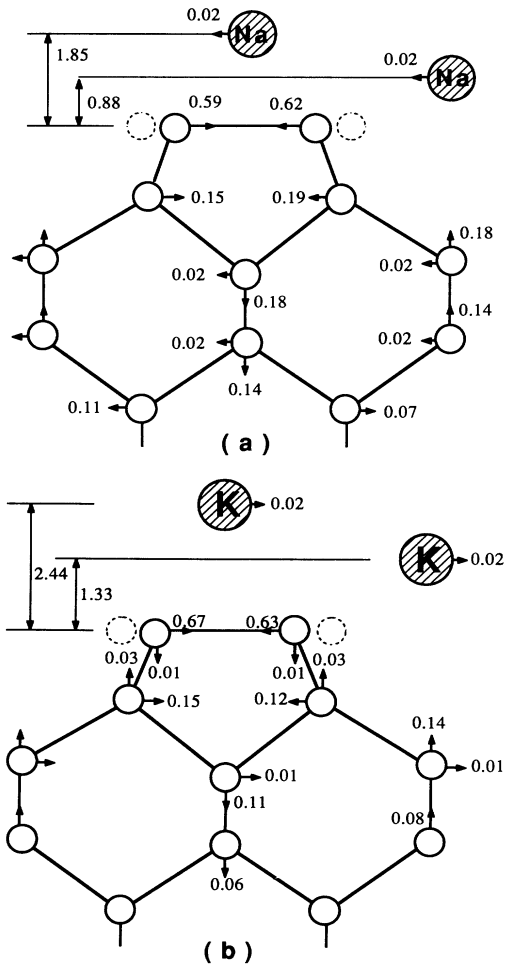

FIG. 4. Side views of the optimized structure for HH-$T3$-site adsorption of (a) Na and (b) K.

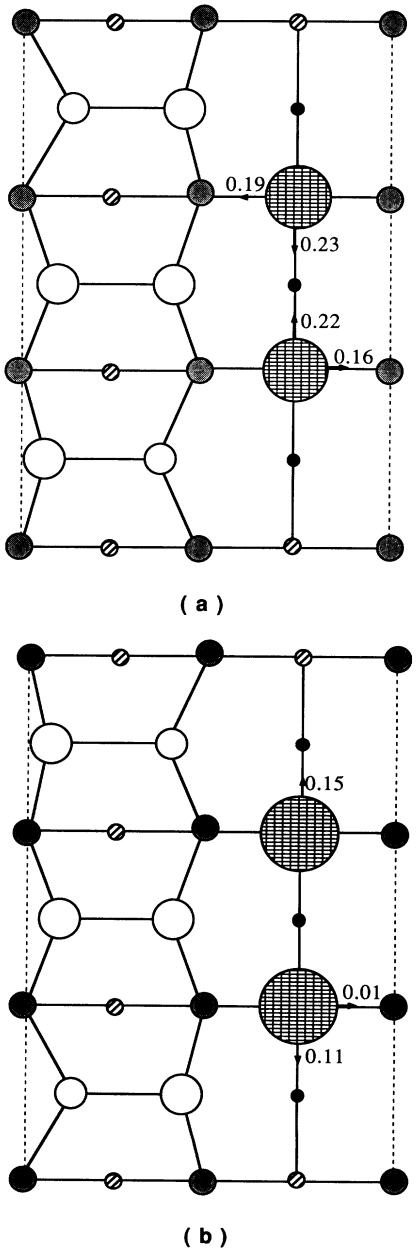

FIG. 5. Top views of the optimized structure at $\Theta=\frac{1}{3}$ for (a) Na and (b) K. The arrows indicate the lateral displacement (in Å) of adatoms from the ideal $T3$ sites.

form substrate potential, the Na-Na distance increases as the coordination number increases. We expect that in the configuration at $\Theta=0.5$, where Na atoms are adsorbed at the $T3$ sites, the Na-Na distance can be expanded to fit the intersite distance. At $\Theta=1.0$, the intersite distance will be rather as expected for Na atoms. These results are qualitatively consistent with the observed Na-Na distance in different environments: It is 3.08 Å for a Na_2 dimer[38] and 3.66 Å for a bulk bcc phase.[31] On the other hand, the K-K distance for a K_2 dimer is 3.91 Å,[38] which is already larger than the intersite distance of the substrate. Therefore, as demonstrated in both Figs. 5(b) and 6(b), K atoms are displaced significantly toward vacant sites. This implies that K atoms are becoming overpopulated as Θ increases.

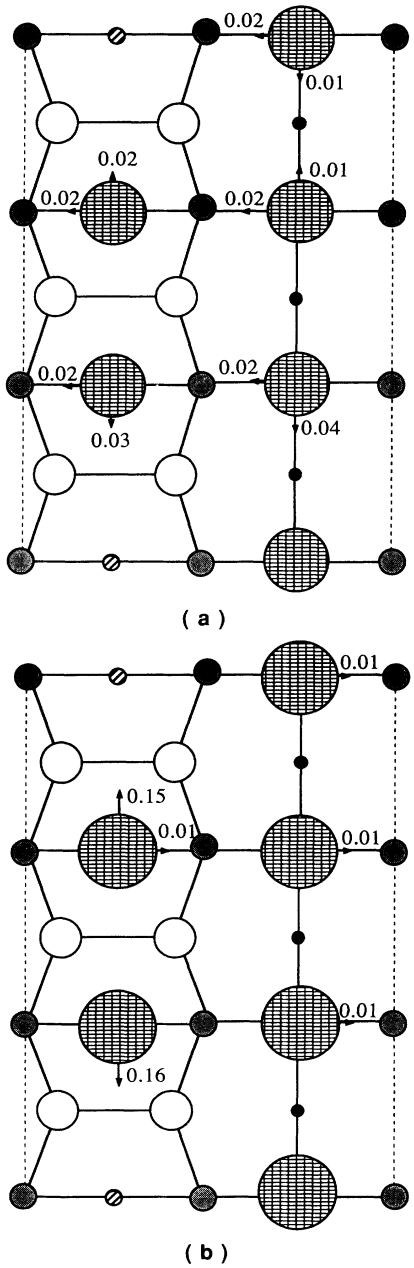

FIG. 6. Top views of the optimized structure at $\Theta=\frac{5}{6}$ for (a) Na and (b) K. The arrows indicate the lateral displacement (in Å) of adatoms from the ideal $T3$ and HH sites.

B. Electronic band structure

Figure 7 shows the band structure for the clean Si(001)-2×1 surface with an asymmetric Si-Si dimer. The two bands S_1 and S_2 are the bonding π band and the antibonding π^* band, respectively. The buckling of the Si-Si dimer enhances the energy separation of S_1 and S_2 by about 0.25 eV compared with the symmetric dimer case. As only the lower half of the S_1-S_2-band complex is occupied, the asymmetric dimer is stabilized by the larger energy separation of S_1 and S_2. In Fig. 7, S_1 and S_2 are virtually nonoverlapping as in other calculations.[39]

The dispersion curves for Na/Si(001) and K/Si(001) systems with $\Theta=0.5$ are shown in Figs. 8 and 9 and the corresponding ones for $\Theta=1.0$ in Fig. 10. The most important aspect in these results is the rigid-band-like shift of the Fermi level as the coverage Θ increases. Irrespective of not only the kind of adatom (Na or K), but also the adsorption site (HH or $T3$), the S_2 band is half-filled for $\Theta=0.5$ and thus the surface is metallic. For $\Theta=1.0$, the surface becomes insulating with a filled S_2 band. If the saturation coverage corresponds to $\Theta=1.0$, the calculated electronic structure is consistent with the observation by Enta *et al.*[9] One may take the apparent filling of the S_2 band by Na and K adsorption as evidence of a donation of the valence electrons from Na or K. Ishida and Terakura[7] gave a detailed discussion on the basic nature of K adsorption and pointed out the important role of the hybridization between the substrate dangling bond and K 4*s* orbital. As in our Figs. 8–10, they also observed that the S_1- and S_2-band energies decrease as Θ increases, although they used a fixed substrate atomic arrangement. They demonstrated that the energy lowering is due to hybridization. Besides, it was shown that the number of electrons inside a sphere centered at K does

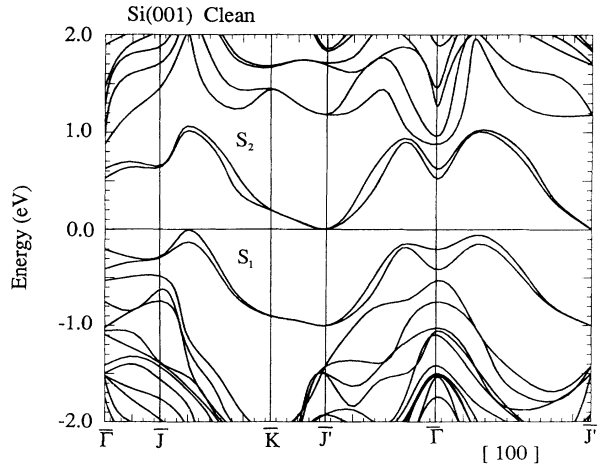

FIG. 7. Band structure of the Si(001)-2×1 clean surface. The splitting of the surface states is due to the interaction between the two surfaces of the Si slab. The origin of the energy is set at the Fermi level.

not change appreciably when an isolated layer is adsorbed on the Si surface. This suggests that the adsorbed K may not be strongly ionized.

In the present results of Figs. 8–10, where the substrate relaxation upon Na or K adsorption is fully taken into account, the energy lowering of the S_1 and S_2 bands is slightly larger and their energy separation is much more reduced than in the results of Ishida and Terakura. The latter is attributed to a significant elongation of the Si-Si dimer caused by Na and K adsorption. The overall trend of the dispersion curve for full coverage of K [Fig. 10(b)] agrees well with the recent angle-resolved photoemission measurement by Abukawa *et al.*[40] In the case of K adsorption, additional surface states S_3 appear for HH-site adsorption. Ishida and Terakura interpreted it as the antibonding state between the bonding π state of the substrate (S_1) and $4s$-$4p_z$ hybrid orbital of K. The absence of S_3 in the case of Na adsorption is due to strong hybridization between S_1 and the $3s$-$3p_z$ hybrid orbital of Na. The S_3 band appears also for Na adsorption if the Na-Si distance is artificially set to the value of the K-Si distance. In the case of $T3$-site adsorption, a surface state corresponding to S_3 is absent for both Na and K. We have also confirmed that such a state appears with a much larger Na-Si distance. This aspect, which implies a stronger interaction between Na (K) and Si, may be responsible for the stronger stabilization of $T3$-site adsorption compared with HH-site adsorption. As there is significant difference in the dispersion curves between Na and K adsorption (Figs. 8–10), an experimental check of this difference is still lacking.

C. Coverage dependence of adsorption energy

The coverage dependence of the adsorption energy is illustrated in Figs. 11(a) and 11(b) for Na and K adsorption, respectively. In the following, $E_{ad}(\Theta_1;\Theta_2)$ denotes the mean adsorption energy per adatom in the coverage between Θ_1 and Θ_2 ($\Theta_2 > \Theta_1$). We first estimate the total energy $E_T(\Theta)$ per surface unit cell for a system with coverage Θ after optimizing the structure. Calculations of $E_T(\Theta)$ for $\Theta=\Theta_1$ and Θ_2 are performed with a common surface unit cell in order to minimize numerical errors caused by k-point sampling and a finite cutoff energy. With N_s denoting the number of the substrate surface atoms in the given surface unit cell, the system with

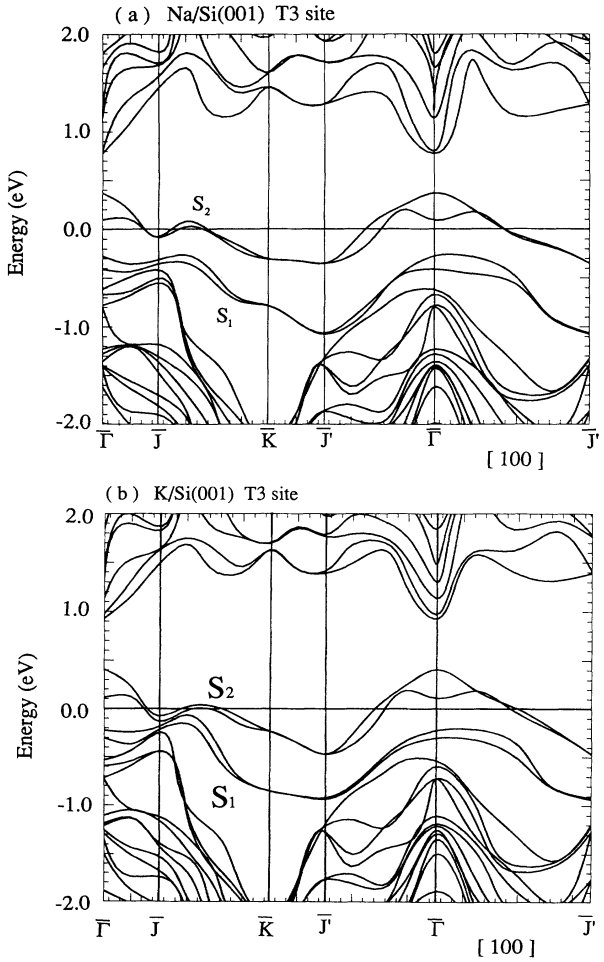

FIG. 8. Band structures of $T3$-site adsorption for (a) Na and (b) K. The splitting of the surface states is due to the interaction between the two surfaces of the slab. The origin of the energy is set at the Fermi level.

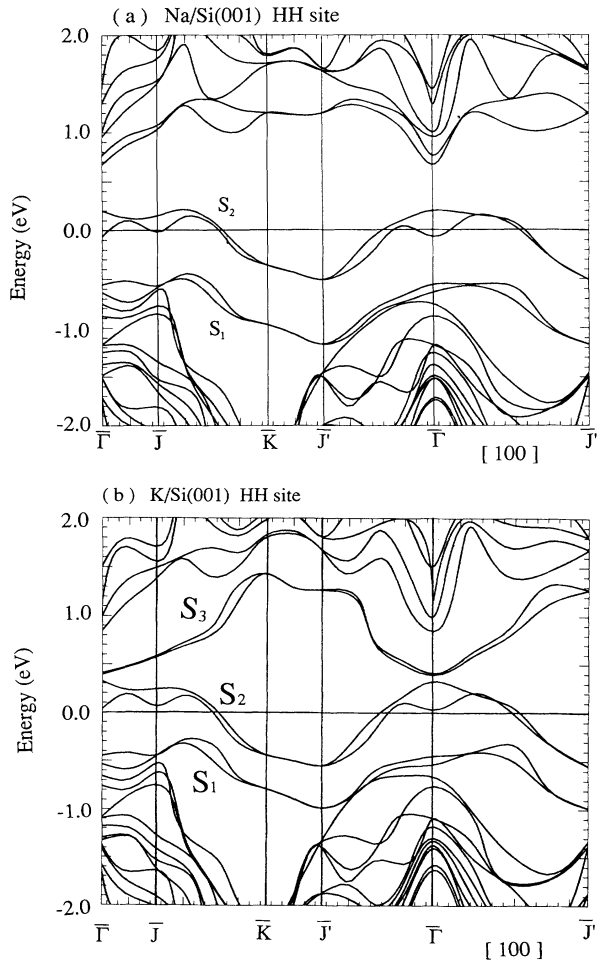

FIG. 9. Band structures of HH-site adsorption for (a) Na and (b) K. The origin of the energy is set at the Fermi level.

$\Theta=\Theta_2$ has more adatoms than that with $\Theta=\Theta_1$ by $N_s(\Theta_2-\Theta_1)$. Therefore, $E_{\rm ad}(\Theta_1;\Theta_2)$ may be estimated as

$$E_{\rm ad}(\Theta_1;\Theta_2)=E_{\rm atom}-\frac{E_T(\Theta_2)-E_T(\Theta_1)}{N_s(\Theta_2-\Theta_1)},$$

where $E_{\rm atom}$ denotes the total energy of a free Na (or K) atom. $E_{\rm atom}$ is estimated by a total-energy calculation for a bcc structure with a large lattice constant of 30.0 a.u. with the same cutoff energy of 6.25 Ry, and the spin-polarization energy (-0.32 eV/atom for Na and -0.25 eV/atom for K) is separately estimated by an all-electron free-atom calculation.

In the course of this analysis, we first noted from $E_T(\frac{1}{2})$ that the adsorption at the $T3$ site is more stable than that at the HH site by about 0.2 eV for Na and 0.4 eV for K. Therefore, the results of $E_{\rm ad}(\Theta_1;\Theta_2)$ shown in Figs. 11(a) and 11(b) were obtained by assuming that Na and K are adsorbed at the HH sites only for $\Theta>0.5$, i.e., after all $T3$ sites are occupied. The results of $E_{\rm ad}(0.0;0.5)$ and $E_{\rm ad}(0.5;1.0)$ for K were presented in the previous work,[21] and it was pointed out that they account well for the observed thermal-desorption spectra.[12] Very good agreement between theory and experiment can be seen more directly in Fig. 11(b), where the experimental estimation[12] is also shown by a dashed curve. The coverage dependence of $E_{\rm ad}$ is not monotonic for Na and K. In the case of K, $E_{\rm ad}(0.5;\frac{5}{6})$ is slightly larger than $E_{\rm ad}(\frac{1}{3};0.5)$. This may imply that before completing $T3$-site adsorption K may be adsorbed at the HH site also. However, a large island will not be formed because $E_{\rm ad}$ starts to decrease again for $\Theta>0.5$. In contrast to K, $E_{\rm ad}(0.5;\frac{5}{6})$ is significantly larger than $E_{\rm ad}(\frac{1}{3};0.5)$ for Na adsorption, and besides, $E_{\rm ad}$ keeps increasing even for $\Theta>0.5$. Our preliminary calculation for Na with $\Theta=\frac{1}{6}$ gives us 2.41 eV as $E_{\rm ad}(0.0;\frac{1}{6})$.[41] As $E_{\rm ad}$ is a decreasing function of Θ at low coverage, Na is adsorbed in such a way that adatoms are mutually separated. However, at a certain critical Θ_c, the mean $E_{\rm ad}$ between $\Theta=0.0$ and Θ_c becomes smaller than $E_{\rm ad}$ at higher coverage. This implies that adsorbed Na will start forming islands at Θ_c.

In order to understand the origin of the different behavior of $E_{\rm ad}$ between Na and K, we try to decompose $E_{\rm ad}$ into various contributions. Conceptually, the adsorption energy consists of the adatom-substrate and adatom-adatom interactions, although such a decomposi-

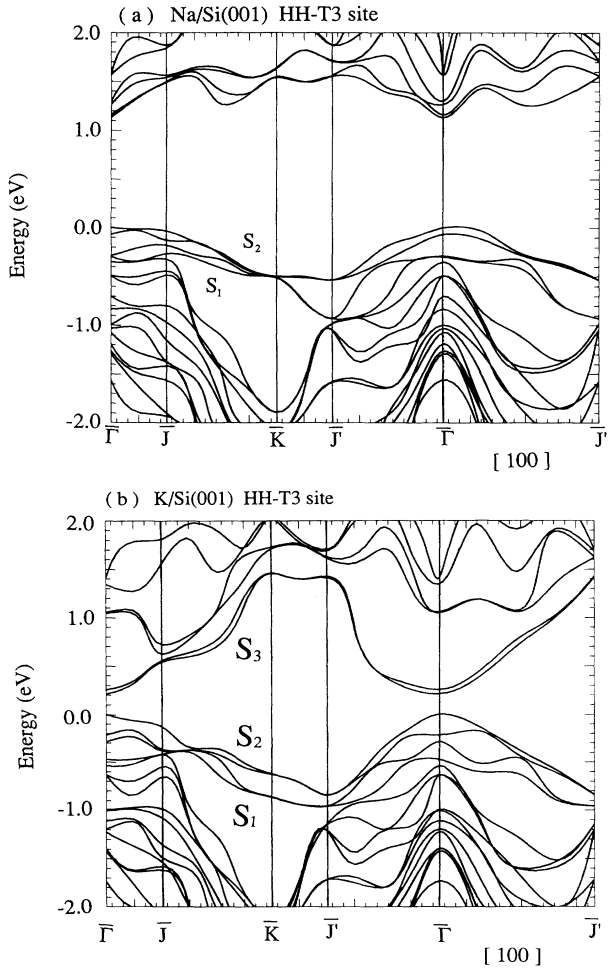

FIG. 10. Band structures of HH-$T3$-site adsorption for (a) Na and (b) K. The origin of the energy is set at the top of the occupied band.

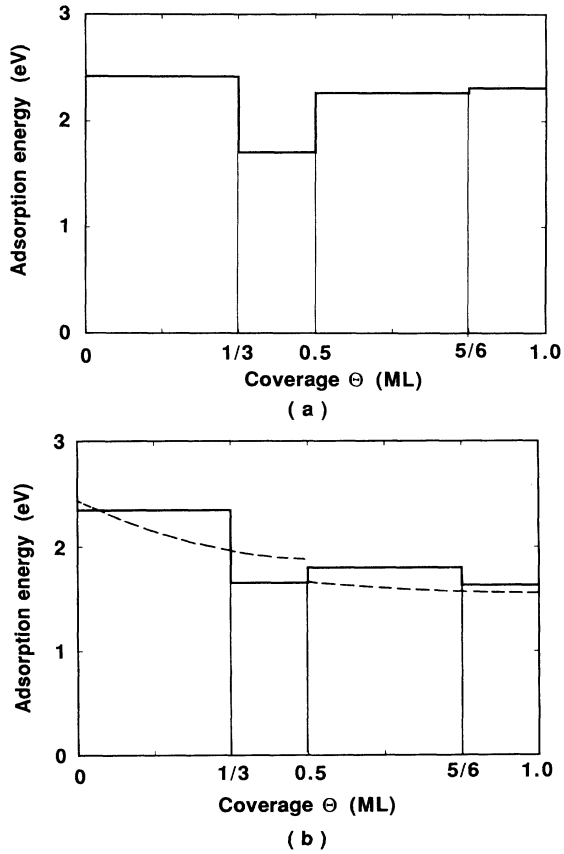

FIG. 11. Coverage dependence of adsorption energy for (a) Na and (b) K. These energies are obtained from the total energies of $\Theta=0.0$, $\frac{1}{3}$, 0.5, $\frac{5}{6}$, and 1.0 systems and a free Na (K) atom. See Sec. III C for the definition of the adsorption energy. The dashed curves denote the experimental estimations (Ref. 12).

tion is not unique. We explain the present convention by taking the analyses of $E_{ad}(0.0;0.5)$ and $E_{ad}(0.5;1.0)$ as examples. We first calculate the energy cost $E_{ad\text{-}sub}$ to separate the adlayer for $\Theta=0.5$ from the substrate, keeping the atomic arrangement in the adlayer fixed, and then calculate the energy cost to make all the atoms in the layer isolated from one another. Neglecting the interchain coupling for $\Theta=0.5$, we call the latter energy cost the intrachain interaction E_{chain}^{intra}. The energy $E_{ad\text{-}sub}$ is then called the adatom-substrate interaction. As for $E_{ad}(0.5;1.0)$, we have to take account of the interchain interaction E_{chain}^{inter}, which is estimated by the following process. After optimizing the adatom arrangement for $\Theta=1.0$, we artificially separate the adlayer from the substrate and then calculate the energy cost per atom, E_{chain}^{inter}, to make the chains isolated from each other. $E_{ad\text{-}sub}$ (0.5;1.0) is the cost in energy to separate the adatoms at the HH sites from the substrate, keeping the two-dimensional atomic arrangement of those adatoms unchanged. The result of such analyses is shown in Figs. 12(a) and 12(b). For the first half-coverage, each of the interaction energies is very similar between Na and K. A slightly larger value of E_{chain}^{intra} for Na than for K reflects the trend in the cohesive energy of elemental metals. However, in the coverage range between $\Theta=0.5$ and 1.0, the situation is significantly different between Na and K. As for Na, $E_{ad\text{-}sub}(0.5;1.0)$ is reduced only slightly compared with $E_{ad\text{-}sub}(0.0;0.5)$, and this small reduction is overcompensated by an appreciable contribution of E_{chain}^{inter}, so that $E_{ad}(0.5;1.0)$ exceeds $E_{ad}(0.0;0.5)$. The reduction of $E_{ad\text{-}sub}$ with an increase of Θ is a rather general phenomenon, being understandable as a consequence of the $1/\sqrt{n}$ scale of strength of a bond, with n denoting the coordination number. On the other hand, $E_{ad\text{-}sub}(0.5;1.0)$ is much smaller than $E_{ad}(0.0;0.5)$ for K, and moreover, E_{chain}^{inter} is also small compared with the value for Na. Such a significant difference in the interaction energies between Na and K in the high-coverage region may be interpreted by the atomic-size difference. In the following we show some evidence that K atoms are contrary to expectations, highly populated at $\Theta=1.0$, while Na atoms are not.

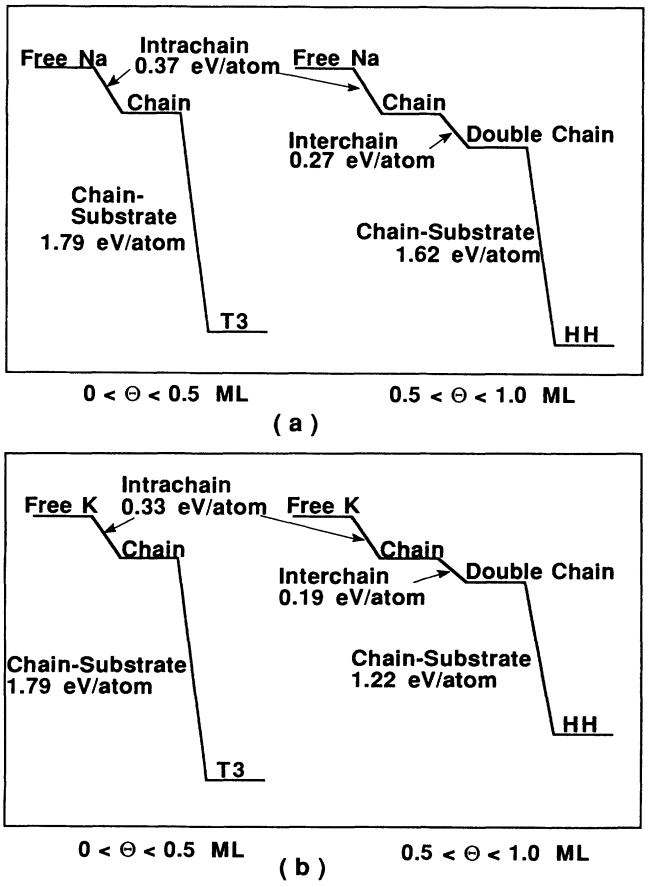

FIG. 12. Decomposition of mean adsorption energies $E_{ad}(0.0;0.5)$ and $E_{ad}(0.5;1.0)$ into some contributions (a) for Na and (b) for K. See Sec. III C for details.

One such evidence can be seen in the optimized structures for $\Theta=1.0$. The height difference between the $T3$ and HH sites for adatoms is 0.96 Å for Na and 1.11 Å for K. Such a corrugation in the adlayer reflects the corrugation of the substrate associated with the dimer hill and trough. If spheres are put on such a surface with corrugation, smaller spheres will follow the corrugation more sensitively than larger spheres. The corrugation in the adlayer mentioned above contradicts this general expectation. A larger corrugation in the K adlayer is a result of relaxation to reduce the strain within the adlayer. More decisive evidence was already given in Figs. 5 and 6. K atoms are forced to be adsorbed up to $\Theta=1.0$ by a strong K-Si interaction.

The coverage dependence of the adsorption energy for Na was measured by Glander and Webb,[42] and their data show qualitatively the same trend as the present results. However, they claim the saturation coverage to be 0.68 rather 1.0. With the absolute coverage Θ_s estimated by them, some strange phenomena were observed. The work function showed an abrupt drop around $\Theta_s=0.68$. The sticking coefficient also went down to zero at $\Theta_s=0.68$, although the adsorption energy showed a still gradual increase there. These experiments were carried out at relatively high temperatures. Another experiment[43] done at 300 K showed also an abrupt drop of the work function at a slightly lower coverage around $\Theta=0.5$. However, annealing at 450 K with a small amount of Na dosing brought the work function back to normal behavior relative to the work-function change. Further deposition of Na at 300 K on this surface again caused an abrupt drop of the work function. The process was repeated several times. The abrupt drop of the work function was attributed to the Smoluchowski mechanism[44] as a result of island formation of the adsorbed Na. Perhaps further study is necessary in order to elucidate these anomalies. We should note that the work-function change for K adsorption does not show such strange behavior.[9]

The present analysis on the coverage dependence of the adsorption energy does suggest island formation for Na, but not for K. However, it is difficult to justify accepting $\Theta=0.68$ as the saturation coverage for Na. We believe that the saturation coverage should be $\Theta=1.0$ for both

Na and K. Some experimental data are available which agree with our claim for K.[13] Similar detailed experiments on Na adsorption are highly desirable.

Before closing this subsection, we would like to mention our study on the cases with $\Theta > 1.0$. By adding another half monolayer on one monolayer of Na, we estimated the adsorption energy and also the change in the work function. $E_{ad}(1.0;1.5)$ drops to 0.83 eV from the value of 2.31 eV for $E_{ad}(5/6;1.0)$. $E_{ad}(1.5;2.0)$ is 1.13 eV. This may suggest that the abrupt drop of the sticking coefficient observed by Glander and Webb should occur at $\Theta = 1.0$. However, we do not have any interpretation on the abrupt drop of the work function. As shown later, the work-function lowering is reduced by forming the second layer of Na.

D. Nature of the bond

As pointed out in Sec. III B, the apparent filling of the S_2 band by alkali-metal adsorption is often regarded as evidence of the ionic nature of the bond between the alkali-metal adatom and substrate. Furthermore, if we plot the total charge density for the alkali-metal-adsorbed Si surface, we can hardly see the electron density around adatoms. This was also regarded as evidence of an ionized state of adatoms. Ishida and Terakura[7] analyzed these problems in detail and concluded that the ionic picture for both of the above aspects is too naive. We would like to make further comments briefly. Let us consider the adsorption problem as an introduction of some perturbing potential to the clean substrate. Alkali-metal atoms add an attractive potential to the system. However, in order to pull down some states in the conduction bands below the Fermi level in the band-gap region, a perturbation should be stronger than some critical value. The perturbation by alkali-metal adsorption is not strong enough to produce new states below the Fermi level. Nevertheless, the S_1 and S_2 states feel the attractive potential and their energies are lowered. The Fermi level is adjusted in order to accommodate additional electrons associated with alkali-metal atoms. An important fact is that the wave functions are modified by the perturbation in such a way that their extension into the vacuum is enhanced. As a result, neutrality of alkali-metal atoms is nearly guaranteed. The basic physics is exactly the same as that discussed many years ago by Terakura and Kanamori[45] for impurities in nickel. We can also interpret the situation in terms of covalency in a linear-combination-of-atomic-orbitals (LCAO) scheme.

A qualitative understanding, as mentioned above, is very important. However, ionicity and covalency, competing factors in the understanding of the nature of the bond, cannot be defined uniquely. They depend on the method of partitioning the charge or, in other words, the choice of basis orbitals. Therefore, we present the charge-density maps in the following in order to provide an objective situation.

Figures 13–15 show difference charge maps for Na adsorption defined as

$$\delta\rho(\mathbf{r}) = \rho_{\mathrm{Na+Si}}(\mathbf{r}) - \rho_{\mathrm{Na}}(\mathbf{r}) - \rho_{\mathrm{Si}}(\mathbf{r}) ,$$

where $\rho_{\mathrm{Na+Si}}$ denotes the charge density for the Na-adsorbed Si surface, ρ_{Na} the one for an isolated Na layer, and ρ_{Si} the one for the substrate. Note that ρ_{Si} is calculated for the atomic arrangement of Si atoms correspond-

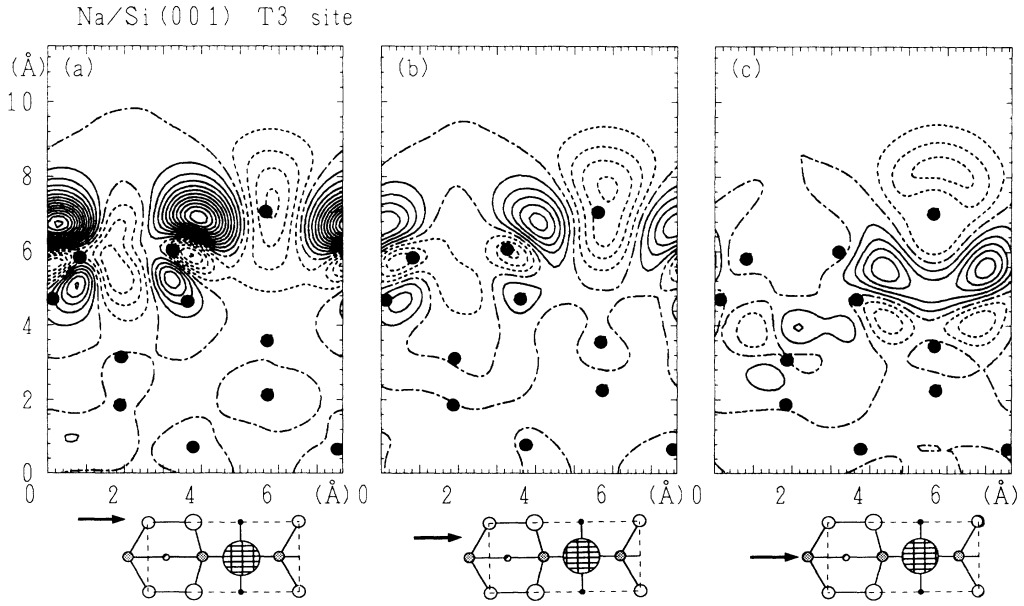

FIG. 13. Difference charge-density maps for Na adsorption with $\Theta = 0.5$ at the $T3$ site within a plane perpendicular to the surface. In each case of (a)–(c), the projection plane is defined so that it contains the arrow shown in each attached small figure. Solid (dashed) curve contour denotes positive (negative) difference charge density. Along the dot-dashed curves, the difference charge density vanishes. The difference between the adjacent contour is 0.0005 a.u. The atomic positions projected onto the plane are denoted by solid circles.

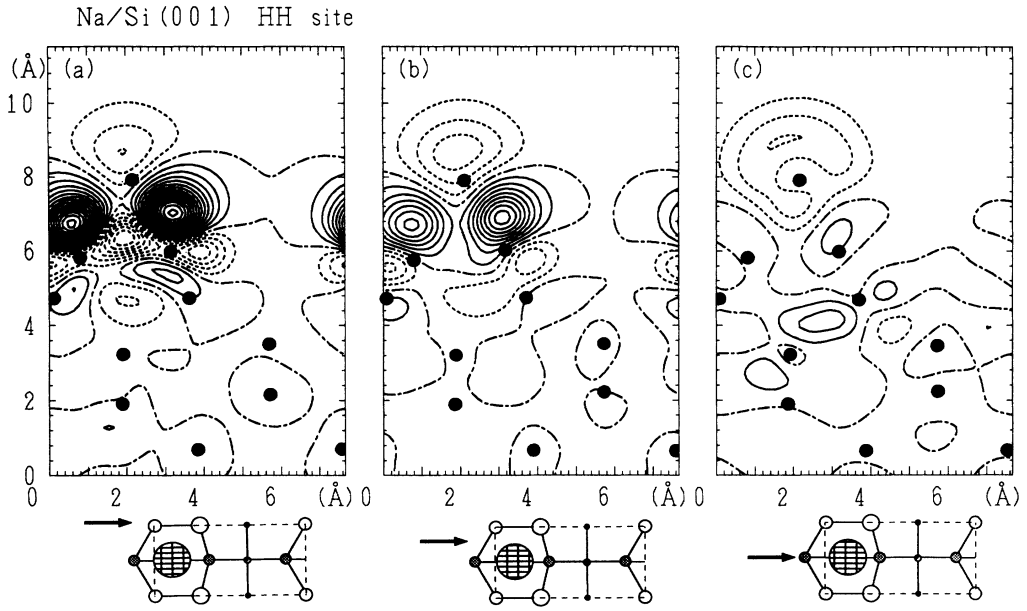

FIG. 14. Difference charge-density maps for Na adsorption with $\Theta=0.5$ at the HH site within a plane perpendicular to the surface.

ing to the optimized structure with Na adsorption. Similar results for the K case are shown in Figs. 16–18. We note the following interesting features in these results.

(1) Only a very weak bond charge is formed between the adatom and substrate within the plane containing the adatom [case (c) in Figs. 16–18]. From the $T3$ site, the nearest substrate Si atoms are in the second layer and the bond charge is formed mostly with these Si atoms. However, as all bonds of these Si are saturated already for the clean surface, the bond distance between the adatom and these Si atoms will be relatively large, as shown in Table II.

(2) The strongest bond charge is formed within the plane containing the Si-Si dimer [case (a) in Figs. 16–18] rather than within the plane halfway between the adatom and Si-Si dimer [case (b) in Figs. 16–18]. This implies that the dangling bond of a surface Si atom interacts most strongly with the metallic bond charge in between the alkali-metal atoms. This may give us some hint of the reason why the $T3$ site is favored rather than the $T4$ site. If the size of the adatom becomes smaller, accumulation of the metallic bond charge will be reduced, and thereby the bond between the metallic bond charge and dangling bond of the substrate will become weaker. In fact, our

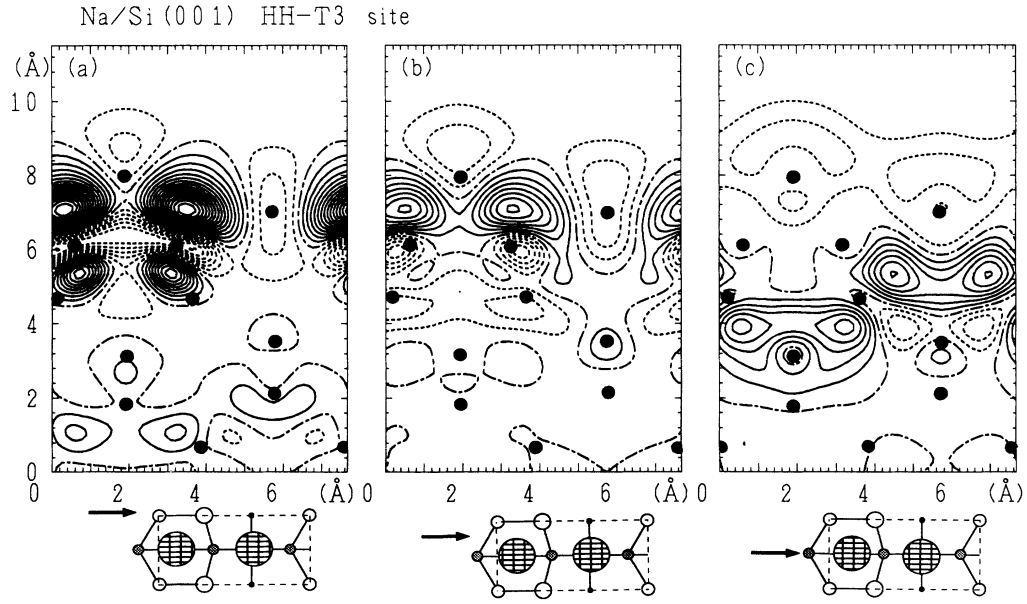

FIG. 15. Difference charge-density maps for Na adsorption with $\Theta=1.0$ at the HH and $T3$ sites within a plane perpendicular to the surface.

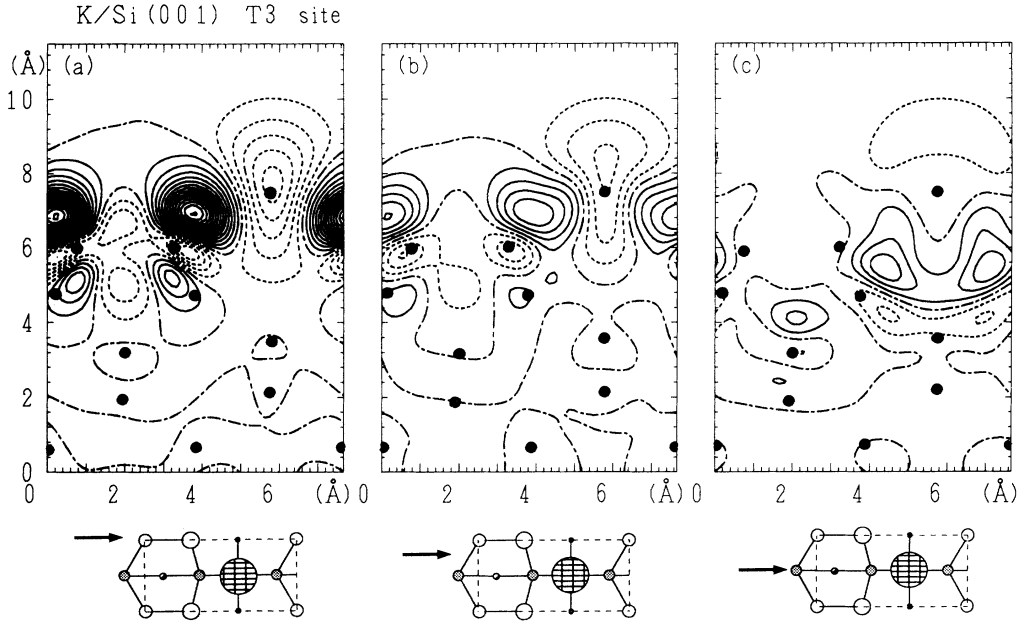

FIG. 16. Difference charge-density maps for K adsorption with $\Theta=0.5$ at the $T3$ site within a plane perpendicular to the surface.

previous study[19] on Na adsorption, which underestimated the Na atomic size by neglecting the PCC, predicted $T4$-site adsorption.

E. Work-function change

Figures 19(a) and 19(b) show the calculated work-function change for Na and K, respectively. As for K, the process of adsorption of the Si(001) surface is rather normal, though the detailed process in very low coverage is not so clear yet. At half coverage, most K atoms are adsorbed along the trough with the rest at the HH site if the substrate temperature is high enough to guarantee thermal equilibrium. Further deposition put K atoms mostly at the HH site. Island formation is improbable. Therefore, we expect that the work-function change for K adsorption will roughly follow the solid line in Fig. 19(b). The experimental data at $\Theta=0.5$ and 1.0 agree quite well with the calculated results.[9]

On the other hand, the growth mode of the adlayer for Na may be rather complicated. First of all, we did not take account of the 3×2 structure. Besides, the possibility of island formation makes the theoretical analysis difficult. Therefore, we cannot compare our results with

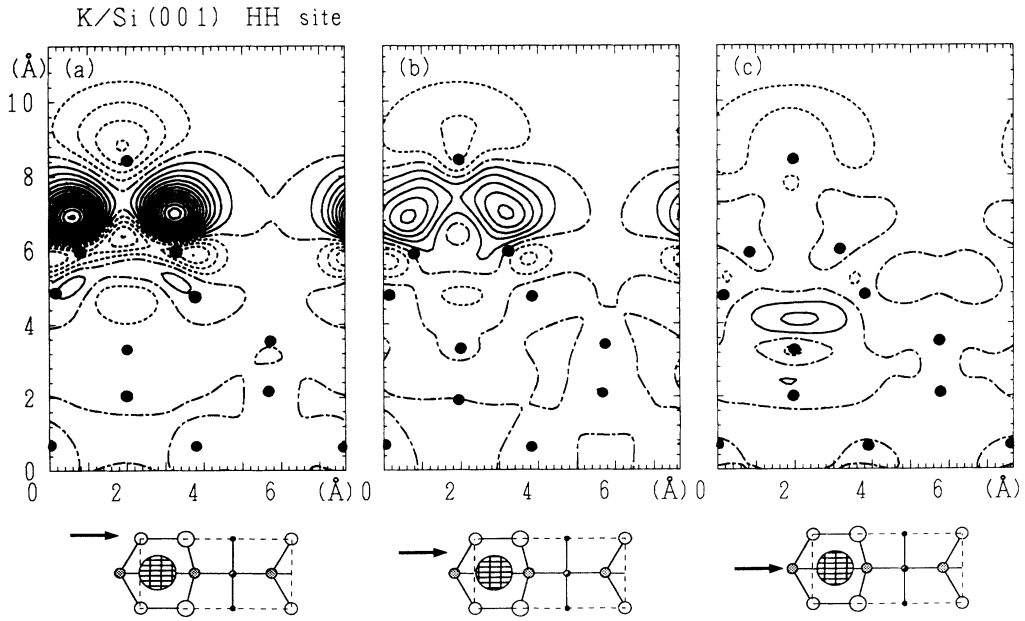

FIG. 17. Difference charge-density maps for K adsorption with $\Theta=0.5$ at the HH site within a plane perpendicular to the surface.

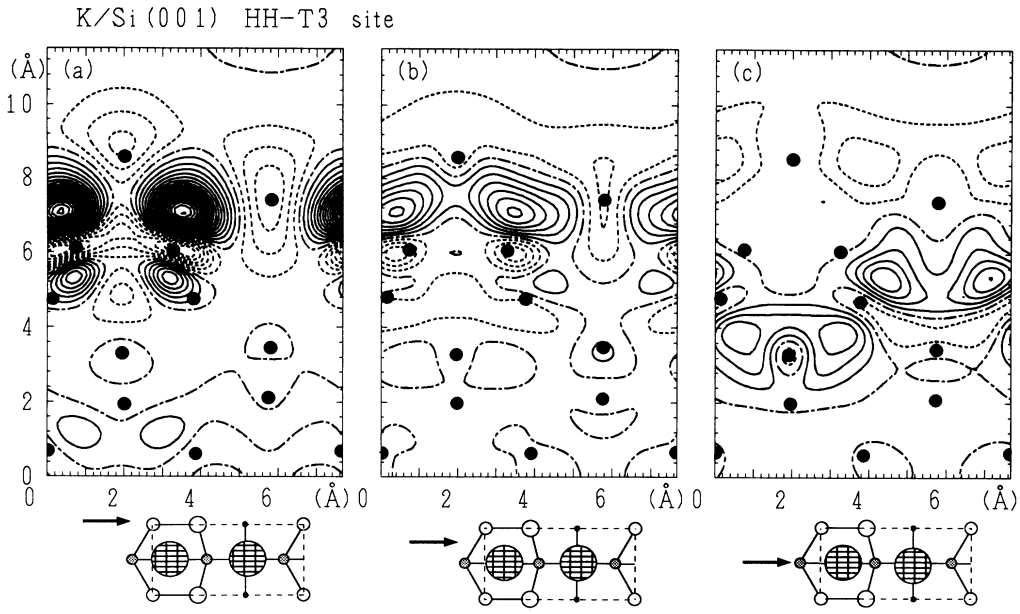

FIG. 18. Difference charge-density maps for K adsorption with $\Theta=1.0$ at the HH and $T3$ sites within a plane perpendicular to the surface.

the experimental data directly. Here we only make some comments on the results shown in Fig. 19(a). At $\Theta=\frac{1}{6}$, we showed the result of our preliminary calculation. We found three locally stable adsorption sites, among which the interdimer bridge site $B2$ is the most stable position, being consistent with the recent scanning-tunneling-microscopy (STM) observations.[46] As Na at the $B2$ site is located far into the vacuum, the induced dipole moment is large to produce a rapid decrease of the work function. More details of the $\Theta=\frac{1}{6}$ case are planned to be presented in a separate paper.[41]

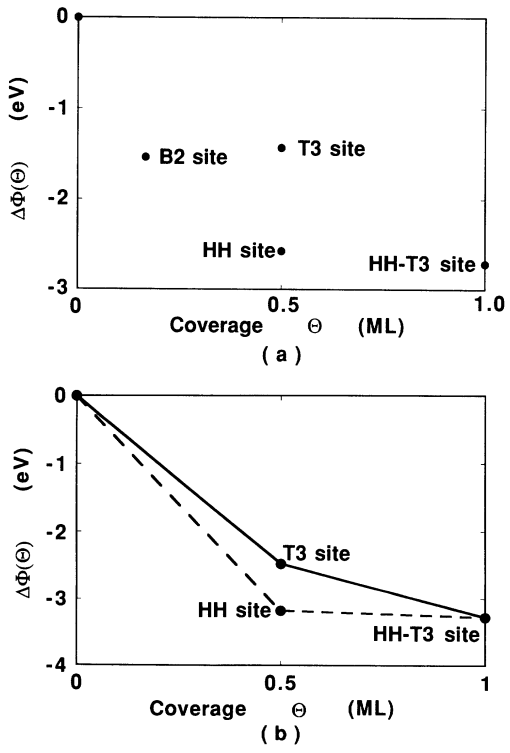

FIG. 19. Work-function change due to (a) Na and (b) K adsorption.

At $\Theta=0.5$, the difference in the work-function change between the HH and $T3$ sites is much larger than that for the K case. This is because Na has a smaller atomic size and can come much closer to the substrate at the $T3$ site compared with K.

At $\Theta=1.0$, the calculated value of the work-function change is about -2.7 eV. It is not clear what experimental situation may correspond to $\Theta=1.0$. However, we would like to point out that the saturated value with annealing the sample[43] agrees well with the above calculated value. We do not have any idea about the experimental value of about -3 eV after the abrupt drop in the work function. The work-function change for $\Theta=1.5$ (2.0) is -1.92 eV (-2.17 eV), being much smaller than -3.0 eV.

IV. CONCLUDING REMARKS

Detailed analyses were performed on the stable atomic arrangement and electronic structure of alkali-metal-Na,K adsorbed Si(001) surfaces. At $\Theta=0.5$, the adsorption along the trough on top of the third-layer Si atoms ($T3$ site) is more stable than the Levine model by about 0.2 eV (0.4 eV) per adatom for Na (K). At $\Theta=1.0$, Na (or K) are adsorbed not only at the $T3$ site, but also at the hollow site along the dimer chain (HH site). The optimized structure for K adsorption at $\Theta=1.0$ agrees well with the experimental analysis.[10] The surface electronic band structure for the full coverage of K also agrees semiquantitatively with the angle-resolved photoemission data.[40]

The present study on the coverage dependence of the adsorption energy E_{ad} has revealed some interesting aspects. First of all, significantly large adsorption energy at high coverage suggests that the saturation coverage will be $\Theta=1.0$ for both Na and K and the calculated result agrees well with the thermal-desorption spectrum for K.[12] E_{ad} decreases nearly monotonically with an increase Θ for K, whereas it starts to increase strongly at certain Θ for Na. The different behavior of E_{ad} between Na and K was attributed to the difference in the atomic size. K atoms are overpopulated within the adlayer, and they are forced to stay on the surface by the strong K-Si interaction. For Na, on the other hand, the intersite distance of 3.84 Å seems to be too large at $\Theta=0.5$, while it becomes more reasonable at $\Theta=1.0$. The increase in the intra-adlayer binding energy overcompensates the decrease in the Na-Si binding energy and results in a net increase of E_{ad} with an increase of Θ. The calculated coverage dependence of E_{ad} for Na agrees qualitatively with the experimental observation.[42] An increase of E_{ad} with Θ may suggest the possibility of island formation.

From the charge-density analysis for $\Theta=0.5$ and 1.0, we noted that a strong bond charge is formed between the dangling bond of a surface Si atom and the metallic bond charge in the adlayer. It was pointed out that this may explain the reason why the $T3$ site rather than the $T4$ site is favored for Na and K adsorption.

Finally, the partial core correction to the pseudopotentials of Na and K is very important in structural optimization. Calculations without the PCC underestimate the bond length significantly and sometimes lead to wrong results for the optimized structure.

In the present paper, we did not take account of the 4×1 and 3×2 structures. The analysis of these will be performed in the near future. Some results in the low-coverage region are planned to be published in a separate paper.

ACKNOWLEDGMENTS

One of the authors (Y.M.) would like to thank Professor M. Nishijima for encouragement during the course of the present work. We thank Dr. R. J. Needs for a comment on the partial core correction to alkali-metal atoms. The numerical calculations were performed at the computer centers of University of Tokyo, Institute for Solid State Physics, and Institute for Molecular Science. A part of the numerical calculation was also performed at the Scientific System Department, Fujitsu Ltd. Kind help in computation from M. Mikami is gratefully acknowledged. This work was partially supported by a Grant-in-Aid for Scientific Research on Priority Areas from the Ministry of Education, Science, and Culture, Japan.

APPENDIX; EFFECTS OF THE PARTIAL CORE CORRECTION ON THE INTERATOMIC DISTANCE

As developed by Louie, Froyen, and Cohen,[22] a partial-core-corrected core pseudopotential is constructed by

$$V^{\rm ion}(r)=V^{ps}(r)-\int\frac{\rho^{va}(r')}{|\mathbf{r}-\mathbf{r}'|}d^3r'-\mu_{\rm xc}[\rho^{pc}(r)+\rho^{va}(r)]\ . \tag{A1}$$

In this equation, V^{ps} is a screened pseudopotential, $\rho^{va}(r)$ an atomic valence charge density, and $\rho^{pc}(r)$ a partial core charge density defined by

$$\rho^{pc}(r)=\begin{cases}A\sin(Br)/r & \text{for } r<r_0\\ \rho^{c}(r) & \text{for } r>r_0\ ,\end{cases} \tag{A2}$$

where $\rho^c(r)$ is a real core charge density, and A and B are chosen so that the amplitude and derivatives of the real and partial core charge densities are identical at $r=r_0$. We choose the core radius r_0 as the radius where the core charge density is twice as large as the valence charge density. The Kohn-Sham equation for band electrons is

$$\left[-\tfrac{1}{2}\nabla^2+\sum_\mu V_\mu^{\rm ion}(\mathbf{r}-\mathbf{R}_\mu)+\int\frac{\rho^{vb}(\mathbf{r})}{|\mathbf{r}-\mathbf{r}|}d^3r+\mu_{\rm xc}\left[\sum_\mu\rho_\mu^{pc}(\mathbf{r}-\mathbf{R}_\mu)+\rho^{vb}(\mathbf{r})\right]\right]\psi_i(\mathbf{r})=\varepsilon_i\psi_i(\mathbf{r})\ , \tag{A3}$$

where μ denotes the μth ion and ρ^{vb} the charge density due to the band electrons. The total energy of this system is given by

$$E=\sum_i^{\rm occupied}\varepsilon_i-\tfrac{1}{2}\int\frac{\rho^{vb}(\mathbf{r})\rho^{vb}(\mathbf{r})}{|\mathbf{r}-\mathbf{r}'|}d^3r\,d^3r'+\tfrac{1}{2}\sum_{\mu\neq\nu}\frac{Z_\mu Z_\nu}{|\mathbf{R}_\mu-\mathbf{R}_\nu|}-\int\mu_{\rm xc}\left[\sum_\mu\rho_\mu^{pc}(\mathbf{r}-\mathbf{R}_\mu)+\rho^{vb}(\mathbf{r})\right]\rho^{vb}(\mathbf{r})d^3r$$
$$+\int\varepsilon_{\rm xc}\left[\sum_\mu\rho_\mu^{pc}(\mathbf{r}-\mathbf{R}_\mu)+\rho^{vb}(\mathbf{r})\right]\left[\sum_\mu\rho_\mu^{pc}(\mathbf{r}-\mathbf{R}_\mu)+\rho^{vb}(\mathbf{r})\right]d^3r\ , \tag{A4}$$

where Z_μ is the number of valence electrons of the μth atom. The Hellmann-Feynman force acting on the μth atom is given by

$$\mathbf{F}_\mu = -\frac{\partial E}{\partial \mathbf{R}_\mu}$$
$$= -\sum_i^{\text{occupied}} \int \psi_i^*(\mathbf{r}) \frac{\partial V_\mu^{\text{ion}}(\mathbf{r}-\mathbf{R}_\mu)}{\partial \mathbf{R}_\mu} \psi_i(\mathbf{r}) d^3r + \sum_{\nu \neq \mu} Z_\mu Z_\nu \frac{(\mathbf{R}_\mu - \mathbf{R}_\nu)}{|\mathbf{R}_\mu - \mathbf{R}_\nu|^3}$$
$$- \int \frac{\partial \rho_\mu^{pc}(\mathbf{r}-\mathbf{R}_\mu)}{\partial \mathbf{R}_\mu} \mu_{\text{xc}} \left[\sum_\mu \rho_\mu^{pc}(\mathbf{r}-\mathbf{R}_\mu) + \rho^{vb}(\mathbf{r}) \right] d^3r \ . \quad \text{(A5)}$$

The first two terms are ordinary contributions to the Hellmann-Feynman force, and the last term is due to the dependence of partial core charge density on the ionic coordinates. We will point out two effects of the PCC. One comes from the potential difference and the other from the Hellmann-Feynman force, i.e., the last term of Eq. (A5).

Let us discuss the former first. The screened pseudopotential contains the exchange-correlation (xc) potential due to the core and atomic valence charge densities:

$$V_{\text{xc},\mu}^{ps} = \mu_{\text{xc}}[\rho_\mu^c + \rho_\mu^{va}] \ . \quad \text{(A6)}$$

A linearization approximation leads to the xc potential in a crystal given by

$$\tilde{V}_{\text{xc}} = \sum_\mu (\mu_{\text{xc}}[\rho_\mu^c + \rho_\mu^{va}] - \mu_{\text{xc}}[\rho_\mu^{va}]) + \mu_{\text{xc}}[\rho^{vb}] \ , \quad \text{(A7)}$$

whereas the actual xc potential should be

$$V_{\text{xc}} = \mu_{\text{xc}} \left[\sum_\mu \rho_\mu^c + \rho^{vb} \right] \ . \quad \text{(A8)}$$

The difference between Eqs. (A7) and (A8) is given by

$$\Delta V_{\text{xc}} = V_{\text{xc}} - \tilde{V}_{\text{xc}}$$
$$= \left[\mu_{\text{xc}} \left[\sum_\mu \rho_\mu^c + \rho^{vb} \right] - \mu_{\text{xc}}[\rho^{vb}] \right]$$
$$- \sum_\mu \left[\mu_{\text{xc}}[\rho_\mu^c + \rho_\mu^{va}] - \mu_{\text{xc}}[\rho_\mu^{va}] \right] \ . \quad \text{(A9)}$$

Because ΔV_{xc} becomes large where the valence charge overlaps with the core charge considerably, we consider the core region of the μth atom. Approximating μ_{xc} with only the exchange contribution,

$$\mu_{\text{xc}}[\rho] \approx -\alpha \rho^{1/3} \ , \quad \text{(A10)}$$

with $\alpha = 2(3/8\pi)^{1/3}$, we obtain

$$\Delta V_{\text{xc}} \approx -\frac{\alpha}{3} \left[\frac{1}{(\rho_\mu^c + \rho_\mu^{va})^{2/3}} - \frac{1}{(\rho_\mu^{va})^{2/3}} \right] \delta\rho \ , \quad \text{(A11)}$$

where $\delta\rho$ is the charge-density difference between band electrons and atomic electrons:

$$\delta\rho - \rho^{vb} - \rho_\mu^{va} \ . \quad \text{(A12)}$$

In the core region that we are interested in, $\delta\rho$ is usually positive because of the tail contribution from the surrounding atoms. Therefore, ΔV_{xc} is positive. It means that the linearized version of the xc potential given by Eq. (A7) is deeper than the actual one given by Eq. (A8) and thereby results in a shrinkage of wave functions and a shrinkage of the interatomic distance. In this respect, the PCC elongates the bond length.

The other contribution of the PCC is the third term of Eq. (A5). ρ^c is spherically symmetric around the center of the core, whereas the center of gravity of the valence charge is displaced into the interatomic bond region. Thus the third term of Eq. (A5) contributes an attractive force.

In the present work, the net effect of the PCC is an elongation of the interatomic distances. However, the third term of Eq. (A5) cannot be neglected. For example, without this term the K-Si bond distance becomes 3.70 Å for $\Theta = 0.5$ ($T3$-site adsorption), being much larger than the corresponding value of 3.39 Å in Table II.

[1]For general references, see articles in *Physics and Chemistry of Alkali Metal Adsorption,* edited by H. P. Bonzel, A. M. Bradshaw, and G. Ertl (Elsevier, Amsterdam, 1989).

[2]H. P. Bonzel, Surf. Sci. Rep. **8**, 43 (1988).

[3]R. W. Gurney, Phys. Rev. **47**, 479 (1935).

[4]E. Wimmer, A. J. Freeman, J. R. Hiskes, and A. M. Karo, Phys. Rev. B **28**, 3074 (1983).

[5]H. Ishida, Phys. Rev. B **42**, 10 899 (1990), and references cited therein.

[6]S. Ciraci and I. P. Batra, Phys. Rev. Lett. **56**, 877 (1986).

[7]H. Ishida and K. Terakura, Phys. Rev. B **40**, 11 519 (1989).

[8]J. D. Levine, Surf. Sci. **34**, 90 (1973).

[9]Y. Enta, T. Kinoshita, S. Suzuki, and S. Kono, Phys. Rev. B **36**, 9801 (1987); Y. Enta, S. Suzuki, S. Kono, and T. Sakamoto, *ibid.* **39**, 5524 (1989).

[10]T. Abukawa and S. Kono, Phys. Rev. B **37**, 9097 (1988).

[11]T. Makita, S. Kohmoto, and A. Ichimiya, Surf. Sci. **242**, 65 (1991).

[12]S. Tanaka, N. Takagi, N. Minami, and M. Nishijima, Phys. Rev. B **42**, 1868 (1990).

[13]A. J. Smith, W. R. Graham, and E. W. Plummer, Surf. Sci. **243**, L37 (1991).

[14]Y. Enta, S. Suzuki, and S. Kono, Surf. Sci. **242**, 277 (1991).

[15]G. S. Glander and M. B. Webb, Surf. Sci. **222**, 64 (1989).

[16]L. Ye, A. J. Freeman, and B. Delley, Phys. Rev. B **39**, 10 144 (1989).

[17]R. Ramirez, Phys. Rev. B **40**, 3962 (1989).

[18]I. P. Batra, Phys. Rev. B **43**, 12 322 (1991).

[19]K. Kobayashi, K. Terakura, and S. Blügel, in *Proceedings of the 13th Taniguchi Symposium on Molecular Dynamics Simulations,* edited by F. Yonezawa (Springer, Berlin, in press).
[20]K. Kobayashi, S. Blügel, H. Ishida, and K. Terakura, Surf. Sci. **242**, 349 (1991).
[21]Y. Morikawa, K. Kobayashi, K. Terakura, and S. Blügel, Phys. Rev. B **44**, 3459 (1991).
[22]S. G. Louie, S. Froyen, and M. L. Cohen, Phys. Rev. B **26**, 1738 (1982).
[23]P. Hohenberg and W. Kohn, Phys. Rev. **136**, B864 (1964).
[24]W. Kohn and L. J. Sham, Phys. Rev. **140**, A1133 (1965).
[25]E. Wigner, Phys. Rev. **46**, 1002 (1934).
[26]G. B. Bachelet, D. R. Hamann, and M. Schlüter, Phys. Rev. B **26**, 4199 (1982).
[27]D. R. Hamann, Phys. Rev. B **40**, 2980 (1989).
[28]L. Kleinman and D. M. Bylander, Phys. Rev. Lett. **48**, 1425 (1982).
[29]R. Car and M. Parrinello, Phys. Rev. Lett. **55**, 2471 (1985).
[30]A. R. Williams and J. Soler, Bull. Am. Phys. Soc. **32**, 562 (1987).
[31]C. Kittle, *Introduction to Solid State Physics,* 5th ed. (Wiley, New York, 1976).
[32]C. S. Barrett, Acta Crystallogr. **9**, 671 (1956).
[33]M. S. Anderson and C. A. Swenson, Phys. Rev. B **28**, 5395 (1983).
[34]M. T. Yin and M. L. Cohen, Phys. Rev. B **24**, 2303 (1981).
[35]B. W. Holland, C. B. Duke, and A. Paton, Surf. Sci. **140**, L269 (1984).
[36]K. Inoue, Y. Morikawa, K. Kobayashi, K. Terakura, and M. Nakayama (unpublished).
[37]M. C. Asensio, E. G. Michel, J. Alvarez, C. Ocal, R. Miranda, and S. Ferrer, Surf. Sci. **211/212**, 31 (1989). The cave site in this work is indeed the $T3$ site in the present paper [E. G. Michel and R. Miranda (private communication)].
[38]K. P. Huber and G. Herzberg, *Molecular Spectra and Molecular Structure IV. Constants of Diatomic Molecules* (Van Nostrand Reinhold, New York, 1979).
[39]Z. Zhu, N. Shima, and M. Tsukada, Phys. Rev. B **40**, 11 868 (1989).
[40]T. Abukawa, T. Kashiwakura, T. Okane, Y. Sasaki, H. Takahashi, Y. Enta, S. Suzuki, S. Kono, S. Sato, T. Kinoshita, A. Kakizaki, T. Ishii, C. Y. Park, S. W. Yu, K. Sakamoto, and T. Sakamoto, Surf. Sci. (to be published).
[41]K. Kobayashi, Y. Morikawa, and K. Terakura (unpublished).
[42]G. S. Glander and M. B. Webb, Surf. Sci. **224**, 60 (1989).
[43]M. Tikhov, G. Boishin, and L. Surnev, Surf. Sci. **241**, 103 (1991).
[44]R. Smoluchowski, Phys. Rev. **60**, 661 (1941).
[45]K. Terakura and J. Kanamori, Prog. Theor. Phys. **46**, 1007 (1971).
[46]T. Hashizume, I. Sumita, Y. Murata, S. Hyodo, and T. Sakurai, J. Vac. Sci. Technol. B **9**, 742 (1991).

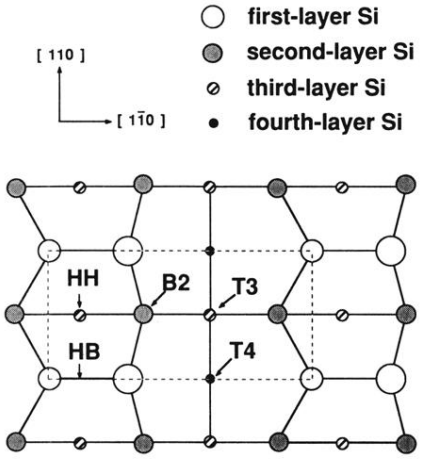

FIG. 1. Top view of the Si(001)-2×1 asymmetric surface. The 2×1 unit cell is indicated by dashed lines. The HH, HB, $T3$, $T4$, and $B2$ sites are indicated. The interdimer bridge site $B2$ is not necessarily just on top of the second-layer Si atom.

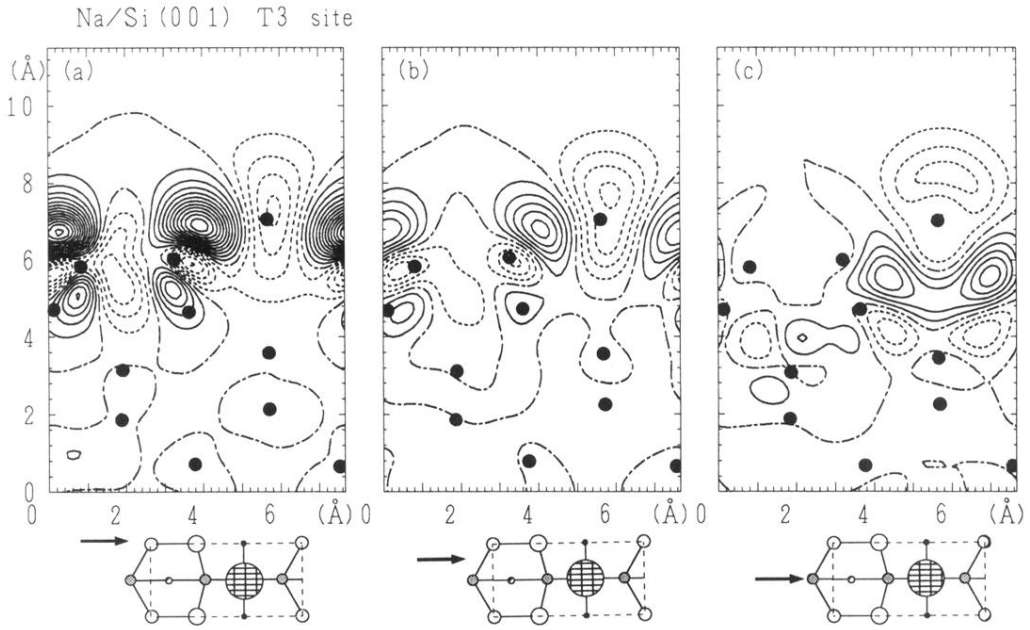

FIG. 13. Difference charge-density maps for Na adsorption with $\Theta=0.5$ at the $T3$ site within a plane perpendicular to the surface. In each case of (a)–(c), the projection plane is defined so that it contains the arrow shown in each attached small figure. Solid (dashed) curve contour denotes positive (negative) difference charge density. Along the dot-dashed curves, the difference charge density vanishes. The difference between the adjacent contour is 0.0005 a.u. The atomic positions projected onto the plane are denoted by solid circles.

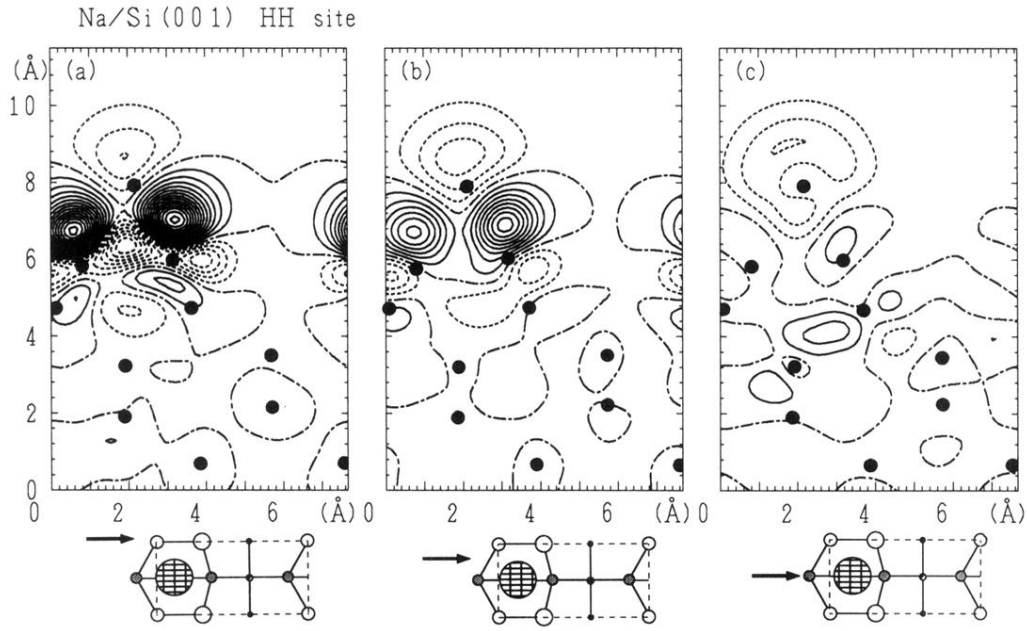

FIG. 14. Difference charge-density maps for Na adsorption with $\Theta=0.5$ at the HH site within a plane perpendicular to the surface.

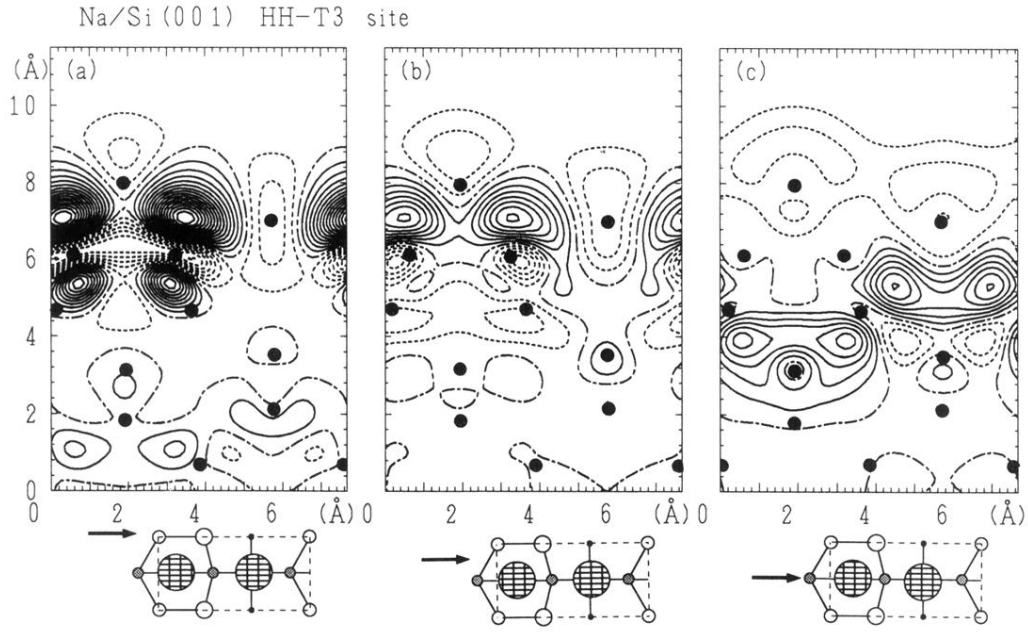

FIG. 15. Difference charge-density maps for Na adsorption with $\Theta = 1.0$ at the HH and $T3$ sites within a plane perpendicular to the surface.

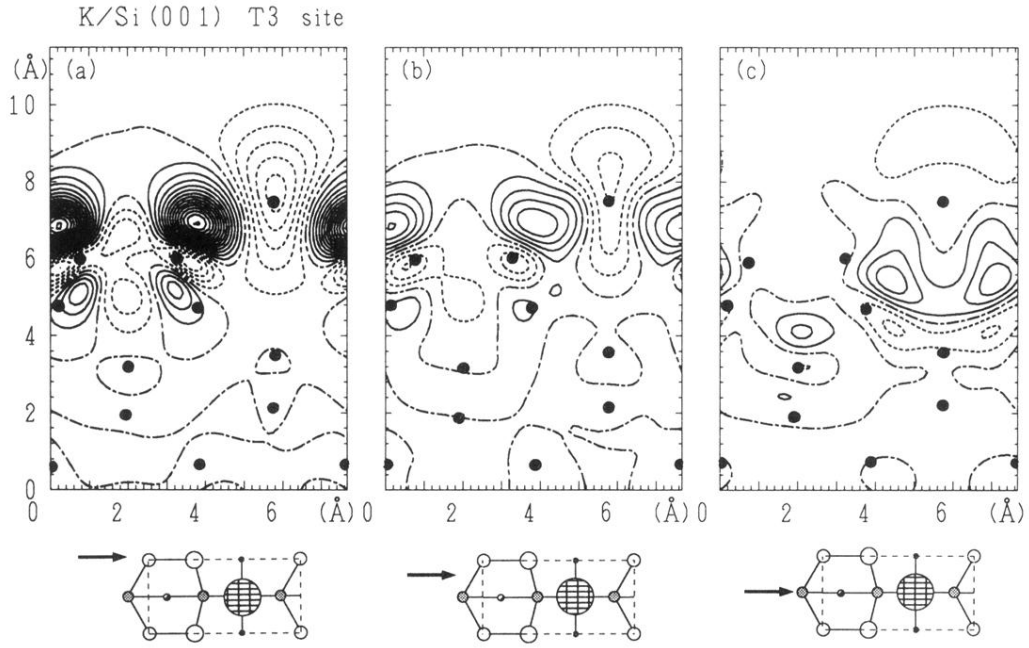

FIG. 16. Difference charge-density maps for K adsorption with $\Theta=0.5$ at the $T3$ site within a plane perpendicular to the surface.

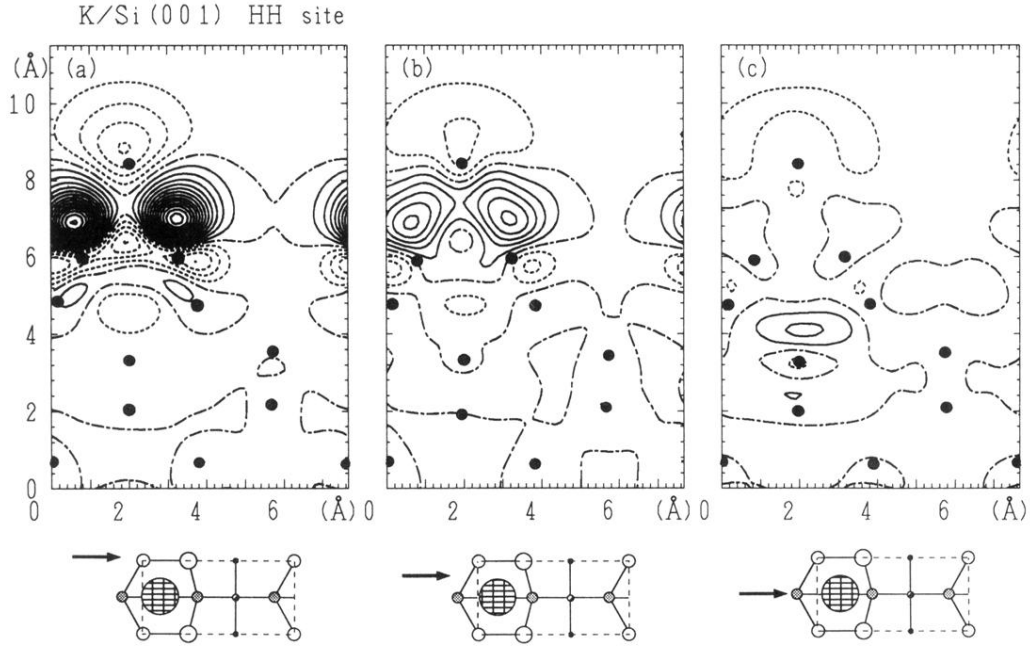

FIG. 17. Difference charge-density maps for K adsorption with $\Theta = 0.5$ at the HH site within a plane perpendicular to the surface.

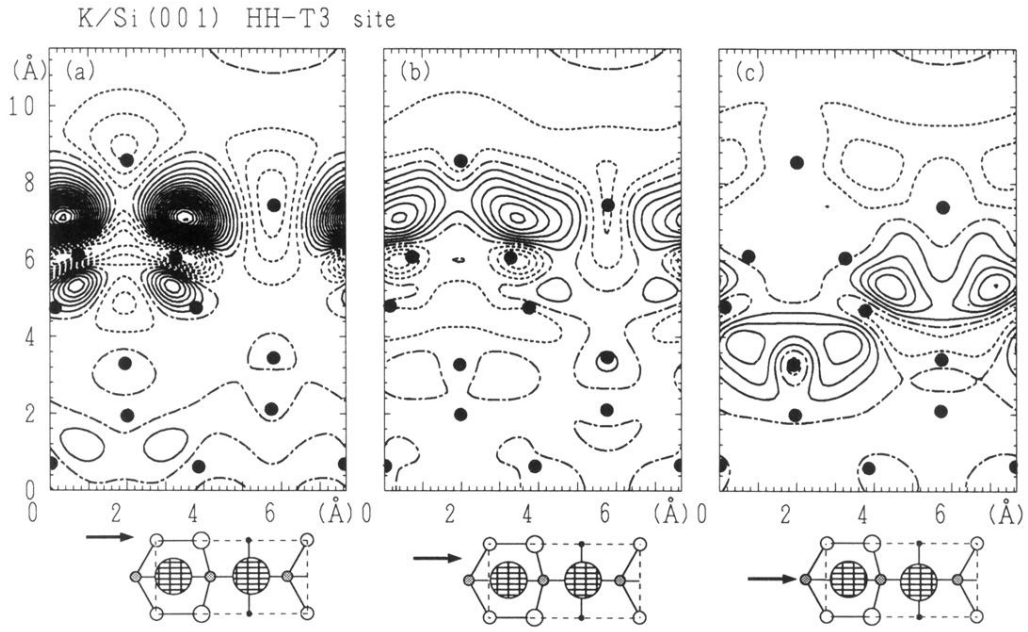

FIG. 18. Difference charge-density maps for K adsorption with $\Theta = 1.0$ at the HH and $T3$ sites within a plane perpendicular to the surface.

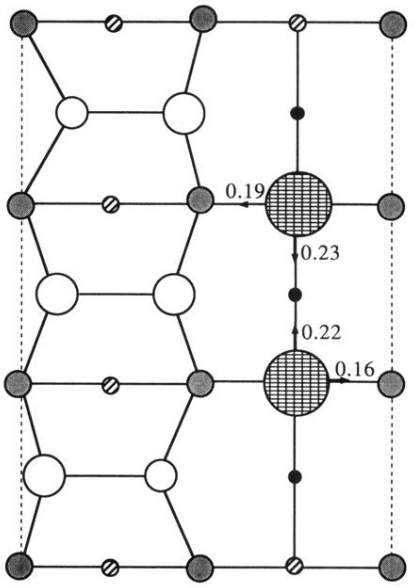

FIG. 5. Top views of the optimized structure at $\Theta = \frac{1}{3}$ for (a) Na and (b) K. The arrows indicate the lateral displacement (in Å) of adatoms from the ideal $T3$ sites.

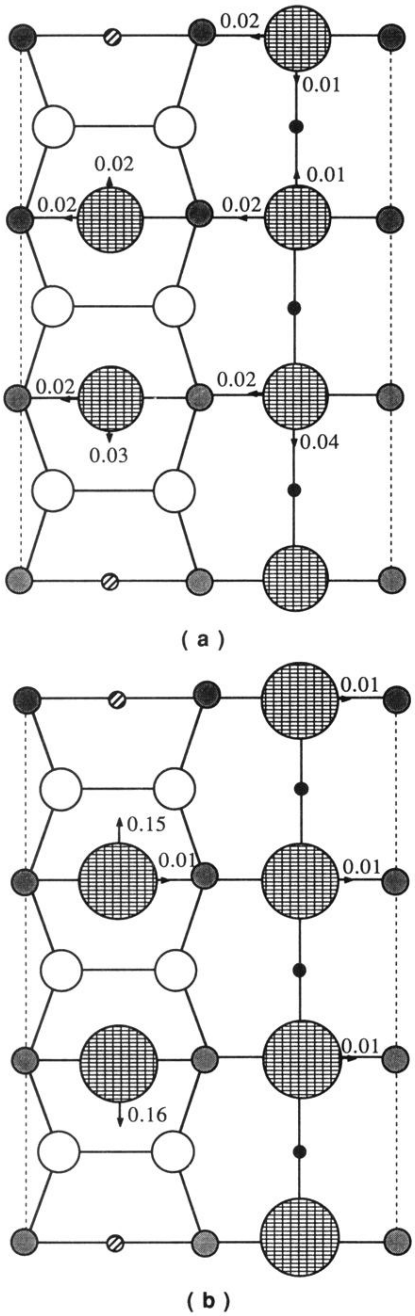

FIG. 6. Top views of the optimized structure at $\Theta = \frac{5}{6}$ for (a) Na and (b) K. The arrows indicate the lateral displacement (in Å) of adatoms from the ideal $T3$ and HH sites.